nature geoscience

ARTICLES

PUBLISHED ONLINE: 22 MAY 2017 | DOI: 10.1038/NGEO2960

Top-of-atmosphere radiative forcing affected by brown carbon in the upper troposphere

Yuzhong Zhang[1], Haviland Forrister[1], Jiumeng Liu[2], Jack Dibb[3], Bruce Anderson[4], Joshua P. Schwarz[5], Anne E. Perring[5,6], Jose L. Jimenez[6,7], Pedro Campuzano-Jost[6,7], Yuhang Wang[1], Athanasios Nenes[1,8,9,10] and Rodney J. Weber[1]*

Carbonaceous aerosols affect the global radiative balance by absorbing and scattering radiation, which leads to warming or cooling of the atmosphere, respectively. Black carbon is the main light-absorbing component. A portion of the organic aerosol known as brown carbon also absorbs light. The climate sensitivity to absorbing aerosols rapidly increases with altitude, but brown carbon measurements are limited in the upper troposphere. Here we present aircraft observations of vertical aerosol distributions over the continental United States in May and June 2012 to show that light-absorbing brown carbon is prevalent in the troposphere, and absorbs more short-wavelength radiation than black carbon at altitudes between 5 and 12 km. We find that brown carbon is transported to these altitudes by deep convection, and that in-cloud heterogeneous processing may produce brown carbon. Radiative transfer calculations suggest that brown carbon accounts for about 24% of combined black and brown carbon warming effect at the tropopause. Roughly two-thirds of the estimated brown carbon forcing occurs above 5 km, although most brown carbon is found below 5 km. The highest radiative absorption occurred during an event that ingested a wildfire plume. We conclude that high-altitude brown carbon from biomass burning is an unappreciated component of climate forcing.

Carbonaceous aerosols, consisting of black carbon (BC) and organic aerosols (OAs), have a significant influence on the climate system. BC is estimated to be an important climate warming agent, next only to CO_2 and CH_4 (ref. 1), because of its absorption of solar radiation. OA has long been thought to primarily scatter sunlight and so cool the climate[1]. However, recent studies report that brown carbon (BrC), a fraction of OA, can also heat the atmosphere by absorbing sunlight, mostly in the lower visible to ultraviolet wavelength range[2,3]. Emitted from incomplete combustion of fuels, especially biomass[4], or produced from secondary formation[5], BrC has been observed in various types of air mass, including fire plumes[6,7], urban air[8,9], continental outflows[3], and in the continental free troposphere[10,11]. BrC concentrations are thought to be highest near biomass-burning sources but then decay over time[12], with small secondary production from known mechanisms[5]. Calculations from both remote sensing observations[13–15] and chemical transport models[16–19] suggest a non-negligible radiative forcing by BrC, ranging from 0.1 to 0.6 W m^{-2} averaged globally, underscoring its potential climate forcing importance. However, these studies have strong differences in their estimates of the distribution and the magnitude of BrC forcing. The discrepancies result from lack of *in situ* BrC data and from uncertainties in both remote sensing and modelling methods.

The climate response to aerosol absorption is found to depend strongly on the altitude of the absorbing aerosols[20–22]. Therefore, information on the vertical distribution of BrC is essential to improve the estimation of its climate impact. In two recent aircraft campaigns, Deep Convective Clouds & Chemistry (DC3) in May–June 2012[23] and Studies of Emissions and Atmospheric Composition, Clouds and Climate Coupling by Regional Surveys (SEAC^{4}RS) in August–September 2013[24], we measured the first altitude-resolved BrC levels, along with many other species. Here, we present results from the unique DC3 and SEAC^{4}RS data sets, with a focus on the radiative impact and sources of BrC in the upper troposphere.

Free tropospheric enhancement of BrC relative to BC

Figure 1a shows the median vertical profile and interquartile ranges of the ratio between absorption coefficients of BrC (b_{BrC}) and BC (b_{BC}) at 365 nm during DC3. Although both b_{BrC} and b_{BC} decrease with altitude, the median b_{BrC}/b_{BC} increases from roughly 0.5 near the boundary layer top (∼2 km) to above unity in the upper troposphere (>9 km), indicating that BrC is more evenly distributed in the tropospheric column than BC (Fig. 1c). Combining DC3 and SEAC^{4}RS aircraft data shows that this feature is prevalent in various regions over the continental US during the warm season and periods of substantial wildfires (Supplementary Fig. 2) in two consecutive years (Supplementary Fig. 1).

Figure 1c plots the computed aerosol absorption optical depth (AAOD, denoted as τ, absorption integrated over the

[1]School of Earth and Atmospheric Sciences, Georgia Institute of Technology, Atlanta, Georgia 30332, USA. [2]Atmospheric Sciences and Global Change Division, Pacific Northwest National Laboratory, Richland, Washington 99352, USA. [3]Earth Systems Research Center, Institute for the Study of Earth, Oceans, and Space, University of New Hampshire, Durham, New Hampshire 03824, USA. [4]Chemistry and Dynamics Branch, NASA Langley Research Center, Hampton, Virginia 23681, USA. [5]Chemical Sciences Division, Earth System Research Laboratory, National Oceanic and Atmospheric Administration, Boulder, Colorado 80305, USA. [6]Cooperative Institute for Research in Environmental Sciences, University of Colorado Boulder, Boulder, Colorado 80309, USA. [7]Department of Chemistry and Biogeochemistry, University of Colorado Boulder, Boulder, Colorado 80309, USA. [8]School of Chemical and Biomolecular Engineering, Georgia Institute of Technology, Atlanta, Georgia 30332, USA. [9]Institute of Environmental Research and Sustainable Development, National Observatory of Athens, Palea Penteli GR-15236, Greece. [10]Institute for Chemical Engineering Science, Foundation for Research and Technology Hellas, Patra GR-26504, Greece. *e-mail: rweber@eas.gatech.edu

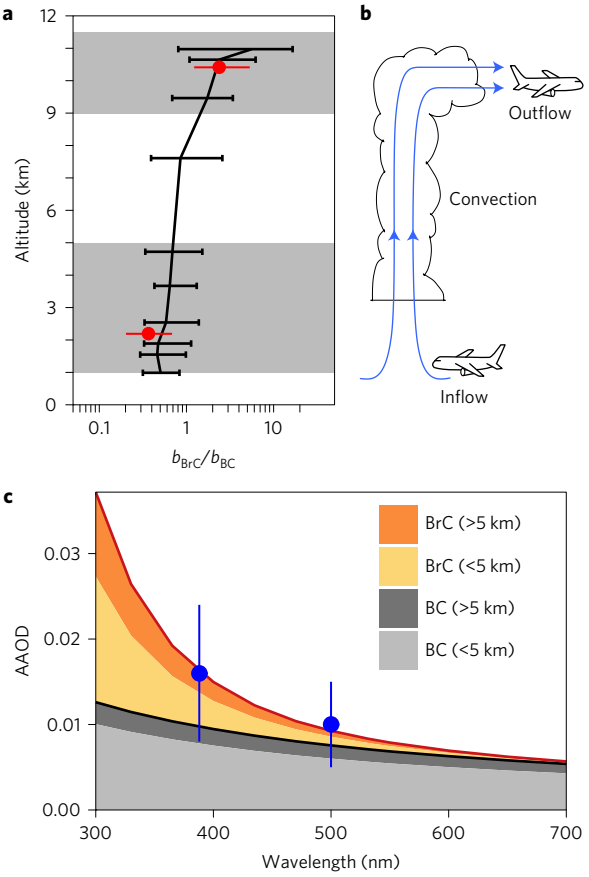

Figure 1 | Aerosol absorption by BC and BrC measured during the DC3 campaign. a, Vertical profile (medians and interquartile) of b_{BrC}/b_{BC} at 365 nm in DC3 (black, all of the data except for biomass-burning samples; red, convective samples). The grey shading shows the altitude ranges of the convective inflow and outflow samples. **b**, Sampling strategy of convection samples in DC3. **c**, AAOD as a function of wavelength, decomposed into those resulting from high-altitude BrC, low-altitude BrC, high-altitude BC and low-altitude BC. The blue dots show the OMI-retrieved AAOD at 388 and 500 nm during DC3 over the sampling region. Vertical lines represent the spatial standard deviation.

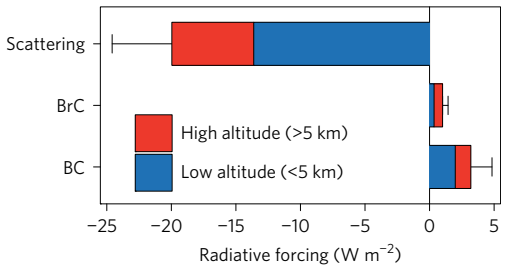

Figure 2 | Instantaneous clear-sky direct radiative forcing estimates of aerosols using the DC3 data. The radiative forcing is decomposed into those from aerosol scattering, BrC absorption and BC absorption. Red and blue bars represent the RF due to aerosols at high (>5 km) and low (<5 km) altitudes. Error bars represent the standard deviations from the Monte Carlo simulations.

layer thickness; see Methods) as a function of wavelength and decomposes τ into that contributed by low-altitude BrC ($\tau_{BrC,<5km}$), low-altitude BC ($\tau_{BC,<5km}$), high-altitude BrC ($\tau_{BrC,>5km}$) and high-altitude BC ($\tau_{BC,>5km}$). Consistent with Fig. 1a, $\tau_{BrC,>5km}$ (3.6×10^{-3}) is 1.8 times $\tau_{BC,>5km}$ (2.0×10^{-3}) at 365 nm. Furthermore, $\tau_{BrC,>5km}$ (1.4×10^{-3}) is about equal to $\tau_{BC,>5km}$ (1.6×10^{-3}) at 435 nm and $\tau_{BrC,>5km}$ (6.9×10^{-4}) is still non-negligible at more than half of $\tau_{BC,>5km}$ (1.4×10^{-3}) up to 500 nm. Thus, BrC absorption at high altitudes is comparable to BC absorption over a substantial range of visible wavelengths and can be optically and radiatively important. Although satellite-retrieved AAOD is generally thought to be uncertain and inferior to *in situ* measurements, it is interesting to note that in the case of DC3, the retrieved AAOD from satellite measurements is in agreement with that derived from *in situ* aircraft measurements at 388 nm and 500 nm (Fig. 1c) over the sampling region (Supplementary Fig. 1a) in May and June of 2012, suggesting that satellite measurements may be sensitive to high-altitude BrC.

Strong warming by upper tropospheric BrC

Figure 2 and Table 1 present radiative transfer calculation results based on DC3 observations (see Methods). For simplicity, the radiative forcing (RF) values shown here are instantaneous clear-sky direct RF values computed at a solar zenith angle of 40°, approximately the mean and median solar zenith angles during the measurement period[10]. Note that the forcing discussed here is instantaneous and hence much larger than the global averages often reported. The overall RF by aerosol (-15.8 ± 4.0 W m^{-2}) is negative (cooling), resulting mainly from aerosol scattering (-20.0 ± 4.6 W m^{-2}). However, the absorption of solar radiation by aerosols reduces this cooling effect by 4.2 ± 1.8 W m^{-2}. Notably, BrC is responsible for 24% of the warming by aerosol absorption, which is generally consistent with previous estimates[16,17].

We then calculated the separate influence of high-altitude (>5 km) and low-altitude (<5 km) aerosols on the clear-sky direct RF (Fig. 2 and Table 1). Because of rapidly decreasing concentrations of total aerosols and BC with altitude, aerosol forcings due to light scattering and BC absorption are considerably smaller at high altitudes (aerosol scattering: -6.4 ± 2.9 W m^{-2}; BC absorption: 1.2 ± 0.8 W m^{-2}) than at low altitudes (aerosol scattering: -13.6 ± 3.2 W m^{-2}; BC absorption: 2.0 ± 1.0 W m^{-2}). In contrast, because of less reduction in BrC with altitude, the RF by BrC at high altitudes (0.65 ± 0.34 W m^{-2}) is about twice that by BrC at low altitudes (0.35 ± 0.16 W m^{-2}) even though the optical depth of high-altitude BrC is only about half of low-altitude BrC (Fig. 1c). As a result, the RF due to BrC contributes ~34% of the RF due to absorbing carbonaceous aerosols at high altitudes, compared with 24% for the whole column and just 15% at low altitudes. In comparison with clear-sky conditions, calculations with DC3 data under global-mean cloudy conditions find a 40% increase in RF due to BrC and 28% increase in RF due to BC, indicating a more significant contribution of BrC if the enhancement of aerosol absorption above clouds is considered (Supplementary Table 2, Supplementary Fig. 3 and Supplementary Text 1). Calculations using SEAC^{4}RS data, a second aircraft campaign a year after DC3, show results similar to DC3, but the RF from high-altitude absorption is less pronounced (Supplementary Table 3 and Supplementary Fig. 4b), very likely to be a result of less convective influence during SEAC^{4}RS (see next section and Supplementary Text 2). High sensitivity of the radiative balance to absorption at high altitudes underscores the importance of understanding the dynamics of absorbing carbonaceous aerosols (that is, BC and BrC) in the upper troposphere.

In addition to the direct radiative effect, high-altitude BrC can also indirectly impact climate through the 'semi-direct effect,' whereby absorption of solar radiation at high altitudes can increase atmospheric stability and subsequently affect convection and cloud formation[21,22]. Incorporation of the absorbing BrC into high convective or cirrus clouds may potentially decrease the reflectivity and lifetime of these clouds, which in turn changes the overall RF[22]. Evaluating the influence of high-altitude BrC on these effects is beyond the scope this study; however, including high-altitude BrC in a chemical transport model should improve estimations of these effects.

Table 1 | Instantaneous clear-sky direct RF estimates of aerosols (scattering, BrC absorption, and BC absorption) over the continental US using the DC3 data.

	Net RF (W m^2)	Absorption (W m^2)			Scattering (W m^2)
		BrC + BC	BrC	BC	
Column	−15.8 ± 4.0	4.2 ± 1.8	1.0 ± 0.4	3.2 ± 1.6	−20.0 ± 4.6
High altitudes (>5 km)	−4.5 ± 2.4	1.9 ± 1.0	0.65 ± 0.34	1.2 ± 0.8	−6.4 ± 2.9
Low altitudes (<5 km)	−11.3 ± 2.9	2.3 ± 1.0	0.35 ± 0.16	2.0 ± 1.0	−13.6 ± 3.2

A campaign-mean solar zenith angle of 40° is used. Mean ± s.d. from the Monte Carlo simulations are reported.

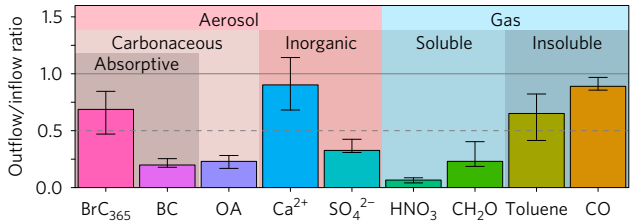

Figure 3 | Measured outflow/inflow ratio of multiple gaseous and aerosol species using the convection samples from DC3. Error bars represent interquartile ranges.

BrC generation and transport by convection

What are the mechanisms responsible for the enhancement of BrC relative to BC in the upper troposphere? To successfully simulate BrC in a chemical transport model, it is critical that this is understood. In May and June of 2012 during the DC3 campaign, the aircraft extensively sampled the inflows and outflows of 12 convective storms (Fig. 1b) (see Methods). These aircraft sampling periods, identified in ref. 25, provide an opportunity to investigate whether convection can serve as a major source of BrC in the upper troposphere. Supplementary Table 1 summarizes information about these convective storm samples. The inflow altitudes are mostly between 1 and 4 km, indicating a boundary layer and possible biomass-burning influence. The outflow altitudes are between 9 and 12 km, which intriguingly coincides with the altitudes where the enhancement of b_{BrC}/b_{BC} occurs (Fig. 1a).

For the 12 convective storms surveyed in DC3, Fig. 3 gives the median and interquartile range for the outflow/inflow ratio of various aerosols and gases. As expected, the behaviours of most gaseous and aerosol species are consistent with their solubility (insoluble CO and toluene have a higher outflow/inflow ratio than soluble CH_2O, HNO_3 and SO_4^{2-}). Notable exceptions are high outflow/inflow ratios (>0.7) for Ca^{2+} and BrC, both of which are often considered to be hydrophilic. The high outflow/inflow ratio for Ca^{2+} has been noted and discussed[25]. Figure 3 also shows that the outflow/inflow ratio for BC is less than 0.25, indicating that a large fraction of BC is removed during convective transport. These results are consistent with the enhancement of b_{BrC}/b_{BC} between 9 and 12 km, suggesting that convection may be an important mechanism for enhancing BrC relative to BC at high altitudes. Also noteworthy is that the median outflow/inflow ratio for OA is only ~0.25, which is similar to that for BC and significantly smaller than that for BrC. This indicates that BrC behaves distinctly from bulk organic aerosols during convection, even though BrC is a component of OA. It should be noted however that the BC and OA instruments sample particles with diameters smaller than approximately 1 μm, whereas the Ca^{2+} and BrC filter-based collection system includes particles up to nominally 4 μm.

One hypothesis that could explain the difference in the outflow/inflow ratio between BrC and BC is the size dependence of wet removal. Using the aerosol size distributions optically measured by a laser aerosol spectrometer during DC3, a previous study found that fine particles (0.1–1 μm diameter) were significantly removed during convective events whereas coarse particles (1–5 μm diameter) were not[25]. Although the reason for this unexpected size dependence was still unknown, it appeared to be consistent with the high outflow/inflow ratio for dust-originated Ca^{2+} (ref. 25). The difference in the outflow/inflow ratio between BrC and BC may reflect the relative enrichment of BrC in the coarse particle mode. If the BrC in convective outflow is associated with larger particles (for example, median size of 2 μm in diameter), the RF by high-altitude BrC absorption reduces from 0.65 to 0.45 W m^{-2}, but the dominance of high-altitude BrC on overall BrC direct radiative forcing remains (see Methods for more discussion on uncertainties). However, this hypothesis cannot be tested without size-resolved BrC measurements, which are unavailable in this data set.

The high outflow/inflow ratio for BrC may also result from BrC formation during convective transport. Field studies have shown evidence that biomass-burning emissions can form BrC in clouds or fogs, a process that can be aided by the pH change in the aqueous phase[26,27]. The cold environment in the outflow region (Supplementary Table 1) may also cause semi-volatile organic compounds, many of which contain chromophores (for example, functionalized polycyclic aromatic compounds[28]), to condense on aerosols. This condensation could be facilitated by ice crystallization during the convective transport. More laboratory and field studies are needed to determine whether these mechanisms are important for BrC formation during convective transport.

Among the 12 convection events in DC3, the highest levels of BrC absorption in the convective outflows were observed in the 22 June event that ingested a wildfire plume[23] (Supplementary Fig. 5). This result appears to be consistent with recent field observations of secondary formation of BrC from biomass-burning emissions in fog water and wet aerosols[27]. Although the detailed mechanism is still unclear, it is likely that biomass-burning emissions make large contributions to not only fresh absorbing aerosols seen in laboratory burning experiments and smoke plume measurements, but also aerosol absorption in the upper troposphere.

Implications

Analysis of DC3 and SEAC^{4}RS data shows that BrC constitutes a significant part of absorbing carbonaceous aerosols, especially at high altitudes. Previous comparisons with remote sensing measurements found that current climate models underestimated AAOD over many regions of the world, although model simulated BC was in reasonable agreement with observations at low altitudes and was even biased high at high altitudes[20,29]. Many factors are very likely to have led to this disagreement[29]. Our results suggest that BrC, which is largely neglected in current climate models, may be a significant factor underlying this disagreement.

Previous studies tend to focus on the optical and radiative effect of primary BrC emitted from fire sources[1,4]. Our study reveals a more dynamic picture of BrC, which undergoes convective transport to high altitudes and affects regional radiative forcing. Previous studies have also shown that BrC freshly emitted from fires bleaches on the timescale of 10 h (ref. 12). In contrast, using measurements in the 'aged' storm outflow sampled one day after the 29 May storm[23], we found that BrC absorption was comparable

between aged and fresh convective outflow (Supplementary Fig. 6), suggesting that BrC at high altitudes persists longer than fresh fire emissions. This finding is significant because horizontal transport is faster in the upper than lower atmosphere. Therefore, high-altitude BrC may disperse into a large area and become an important climate factor on a regional scale (Supplementary Fig. 7). The data point to biomass burning as an important source of BrC, implying that BrC will play an increasing role in the planetary radiative balance due to expected intensifying future wildfire emissions[30].

Methods

Methods, including statements of data availability and any associated accession codes and references, are available in the online version of this paper.

Received 21 December 2016; accepted 21 April 2017; published online 22 May 2017

References

1. Myhre, G. *et al*. in *Climate Change 2013: The Physical Science Basis* (eds Stocker, T. F. *et al*.) 659–740 (IPCC, Cambridge Univ. Press, 2013).
2. Kirchstetter, T. W., Novakov, T. & Hobbs, P. V. Evidence that the spectral dependence of light absorption by aerosols is affected by organic carbon. *J. Geophys. Res.* **109,** D21208 (2004).
3. Alexander, D. T. L., Crozier, P. A. & Anderson, J. R. Brown carbon spheres in East Asian outflow and their optical properties. *Science* **321,** 833–836 (2008).
4. Saleh, R. *et al*. Brownness of organics in aerosols from biomass burning linked to their black carbon content. *Nat. Geosci.* **7,** 647–650 (2014).
5. Zhang, X. *et al*. Light-absorbing soluble organic aerosol in Los Angeles and Atlanta: a contrast in secondary organic aerosol. *Geophys. Res. Lett.* **38,** L21810 (2011).
6. Kirchstetter, T. W. & Thatcher, T. L. Contribution of organic carbon to wood smoke particulate matter absorption of solar radiation. *Atmos. Chem. Phys.* **12,** 6067–6072 (2012).
7. Liu, X. *et al*. Agricultural fires in the southeastern US during SEAC^{4}RS: emissions of trace gases and particles and evolution of ozone, reactive nitrogen, and organic aerosol. *J. Geophys. Res.* **121,** 7383–7414 (2016).
8. Hecobian, A. *et al*. Water-Soluble Organic Aerosol material and the light-absorption characteristics of aqueous extracts measured over the Southeastern United States. *Atmos. Chem. Phys.* **10,** 5965–5977 (2010).
9. Liu, J. *et al*. Size-resolved measurements of brown carbon in water and methanol extracts and estimates of their contribution to ambient fine-particle light absorption. *Atmos. Chem. Phys.* **13,** 12389–12404 (2013).
10. Liu, J. *et al*. Brown carbon in the continental troposphere. *Geophys. Res. Lett.* **41,** 2191–2195 (2014).
11. Liu, J. *et al*. Brown carbon aerosol in the North American continental troposphere: sources, abundance, and radiative forcing. *Atmos. Chem. Phys.* **15,** 7841–7858 (2015).
12. Forrister, H. *et al*. Evolution of brown carbon in wildfire plumes. *Geophys. Res. Lett.* **42,** 4623–4630 (2015).
13. Arola, A. *et al*. Inferring absorbing organic carbon content from AERONET data. *Atmos. Chem. Phys.* **11,** 215–225 (2011).
14. Chung, C. E., Ramanathan, V. & Decremer, D. Observationally constrained estimates of carbonaceous aerosol radiative forcing. *Proc. Natl Acad. Sci. USA* **109,** 11624–11629 (2012).
15. Wang, X. *et al*. Deriving brown carbon from multi-wavelength absorption measurements: method and application to AERONET and surface observations. *Atmos. Chem. Phys. Discuss.* **2016,** 1–33 (2016).
16. Feng, Y., Ramanathan, V. & Kotamarthi, V. R. Brown carbon: a significant atmospheric absorber of solar radiation? *Atmos. Chem. Phys.* **13,** 8607–8621 (2013).
17. Wang, X. *et al*. Exploiting simultaneous observational constraints on mass and absorption to estimate the global direct radiative forcing of black carbon and brown carbon. *Atmos. Chem. Phys.* **14,** 10989–11010 (2014).
18. Jo, D. S., Park, R. J., Lee, S., Kim, S. W. & Zhang, X. A global simulation of brown carbon: implications for photochemistry and direct radiative effect. *Atmos. Chem. Phys.* **16,** 3413–3432 (2016).
19. Saleh, R. *et al*. Contribution of brown carbon and lensing to the direct radiative effect of carbonaceous aerosols from biomass and biofuel burning emissions. *J. Geophys. Res.* **120,** 10285–10296 (2015).
20. Hodnebrog, Ø, Myhre, G. & Samset, B. H. How shorter black carbon lifetime alters its climate effect. *Nat. Commun.* **5,** 5065 (2014).
21. Ban-Weiss, G. A., Cao, L., Bala, G. & Caldeira, K. Dependence of climate forcing and response on the altitude of black carbon aerosols. *Clim. Dynam.* **38,** 897–911 (2012).
22. Koch, D. & Del Genio, A. D. Black carbon semi-direct effects on cloud cover: review and synthesis. *Atmos. Chem. Phys.* **10,** 7685–7696 (2010).
23. Barth, M. C. *et al*. The deep convective clouds and chemistry (DC3) field campaign. *Bull. Am. Meteorol. Soc.* **96,** 1281–1309 (2015).
24. Toon, O. B. *et al*. Planning, implementation, and scientific goals of the Studies of Emissions and Atmospheric Composition, Clouds and Climate Coupling by Regional Surveys (SEAC^{4}RS) field mission. *J. Geophys. Res.* **121,** 4967–5009 (2016).
25. Corr, C. A. *et al*. Observational evidence for the convective transport of dust over the central United States. *J. Geophys. Res.* **121,** 1306–1319 (2016).
26. Desyaterik, Y. *et al*. Speciation of "brown" carbon in cloud water impacted by agricultural biomass burning in eastern China. *J. Geophys. Res.* **118,** 7389–7399 (2013).
27. Gilardoni, S. *et al*. Direct observation of aqueous secondary organic aerosol from biomass-burning emissions. *Proc. Natl Acad. Sci. USA* **113,** 10013–10018 (2016).
28. Laskin, A., Laskin, J. & Nizkorodov, S. A. Chemistry of atmospheric brown carbon. *Chem. Rev.* **115,** 4335–4382 (2015).
29. Koch, D. *et al*. Evaluation of black carbon estimations in global aerosol models. *Atmos. Chem. Phys.* **9,** 9001–9026 (2009).
30. Liu, Y., Stanturf, J. & Goodrick, S. Trends in global wildfire potential in a changing climate. *For. Ecol. Manage.* **259,** 685–697 (2010).

Acknowledgements

All data used in this paper were collected as part of the NASA DC3 and SEAC^{4}RS missions and became available to the general public on 15 October 2014 through the NASA data archive. Georgia Tech researchers were funded through NASA Radiation Sciences Program grant NNX14AP74G. NASA Tropospheric Composition Program supported J.D. through grant NNX12AB80G, and P.C.-J. and J.L.J. through grants NNX12AC03G and NNX15AT96G. H.F. was supported by the National Science Foundation Graduate Research Fellowship under Grant No. DGE-1650044. The authors thank G. Chen and C. Corr for discussion with Y.Z.

Author contributions

Y.Z., Y.W., A.N. and R.J.W. designed the study. Y.Z. performed the analysis and calculation. J.L., J.D., B.A., J.P.S., A.E.P., J.L.J., P.C.-J. and R.J.W. conducted and analysed the aircraft measurements. Y.Z., H.F., Y.W., A.N. and R.J.W. discussed the results. Y.Z., Y.W., A.N. and R.J.W. wrote the paper. J.L.J., J.L., H.F., J.D. and J.P.S. provided input on the paper for revision before submission.

Additional information

Supplementary information is available in the online version of the paper. Reprints and permissions information is available online at www.nature.com/reprints. Publisher's note: Springer Nature remains neutral with regard to jurisdictional claims in published maps and institutional affiliations. Correspondence and requests for materials should be addressed to R.J.W.

Competing financial interests

The authors declare no competing financial interests.

Methods

Aircraft measurements. During the DC3 campaign in May and June 2012, the NASA DC-8 research aircraft was deployed to collect a comprehensive suite of gas and aerosol data in the troposphere (0.5–12 km) over the central US. Ref. 23 describes the scientific goals and the sampling strategy of the campaign.

During the DC3 campaign, 541 filter samples (Teflon EMD Millipore, 1 μm pore size, 90 mm diameter) were collected. Most of the samples have a 5 min integration time during level flight legs. These filters were stored below freezing in the dark before analysis and were extracted in water to quantify soluble species such as Ca^{2+}, SO_4^{2-} and NO_3^- using ion chromatography (Dionex)[25] and light absorption coefficients of BrC. The filter was then re-extracted in methanol and the light absorption coefficients of BrC measured again[8]. Ion concentrations and BrC light absorption coefficients were corrected for filter artefacts using filter blanks collected during each flight. The sum of water and methanol light absorption is taken as the total solution absorption by BrC ($b_{SE,BrC}$), which is the basis for the BrC light absorption measurements of this study. A multiplication factor of 2 was applied to convert the solution absorption to aerosol absorption (b_{BrC}) (refs 9,10). This factor (f_{BrC}) is mainly a result of enhanced particle absorption efficiency by particles in the Mie regime versus absorption by chromophores (molecules) in the bulk liquid extract, and therefore a function of BrC aerosol size distributions. Closure analyses in multiple field studies all indicate that the factor is close to 2 (refs 7,9,10,31), which is consistent with a median particle diameter of 0.5 μm. If BrC-containing particles are larger than this, the factor will be smaller. We discuss the influence of an increased median diameter of BrC on radiative forcing in the main text where we hypothesize that one cause for BrC enhancements relative to BC when passing through convection may be due to differences in size distributions.

The accumulation-mode mass concentration of BC was measured by a single-particle soot photometer (SP2) (ref. 32) and submicrometre particulate mass loading of OA was measured by an aerodyne aerosol mass spectrometer[33]. Particle light absorption coefficients at 400, 550 and 660 nm wavelength were measured by a particle soot absorption photometer (PSAP)[34,35]. Light scattering coefficients of dry particles at 450, 550 and 700 nm wavelength were measured by a TSI-3563 Nephelometer[36]. Readers are referred to ref. 23 for more information about the DC3 payload, including additional instruments whose data are used here. To support our conclusions, we also use some data from SEAC^{4}RS. The payload in SEAC^{4}RS was largely identical to that in DC3 and a description can be found in ref. 24.

Convective inflow and outflow samples. One of the major scientific objectives of DC3 was to study the influence of mid-latitude convective clouds on the dynamics and chemistry in the upper troposphere[23,25,37,38]. The aircraft purposefully sampled the inflow and outflow of convective storms. The inflow and outflow samples of 12 storms, mainly over the states of Colorado and Oklahoma, were identified in previous studies[25]. The inflow samples were determined on the basis of video record, flight report and radar, and the outflow samples were determined on the basis of ice water content and NO concentrations[25]. Supplementary Table 1 summarizes the information (date, time, altitude and outflow temperature) regarding these inflow and outflow samples.

To understand the effect of convection, we computed the ratio between the outflow and the inflow samples for multiple gaseous and aerosol species, including BrC and BC. Note that the apparent outflow/inflow ratio presented in this study accounts for the influence of convective transport, entrainment and, for some species, chemical production and cloud processing. The influence of entrainment is estimated to 7.3 ± 3.3% km^{-1} (ref. 37). We also assume that the inflow and outflow samples represent the same air mass before and after each convective transport. The assumption is supported by similar *n*-pentane to *i*-pentane ratios between the inflow and the outflow samples[25].

Radiative forcing calculation. On the basis of the measurements obtained during DC3 and SEAC^{4}RS, we conducted a series of radiative transfer calculations using the Santa Barbara DISORT Atmospheric Radiative Transfer (SBDART) model[39] to compute the short-wave (0.25–4 μm) radiative forcing (RF) at the top of the troposphere. All of the DC3 data were used in our calculation except for biomass-burning plume samples[10]. Therefore, the results should be interpreted as a regional background, which was probably influenced by wildfires (Supplementary Fig. 2). A similar analysis was done for the SEAC^{4}RS data, which were used only to support the findings from the DC3 study; the predicted radiative results are not reported in the main text.

We employ the Monte Carlo method to account for the uncertainty in the parameters and variation in the measurements. To compute the input to SBDART, we first bin the DC3 samples into 10 altitude bins each containing approximately 10% of the data. For each Monte Carlo run, we generate a composite vertical profile by randomly picking one sample from each bin. We used the measurements in this composite vertical profile to compute the altitude- and wavelength-dependent partial aerosol optical depth and single scattering albedo (SSA). This aerosol optical information was then used as input to SBDART.

The partial aerosol optical depth ($\tau(h,\lambda)$) at altitude h and wavelength λ is contributed by aerosol scattering and absorption by BC and BrC:

$$\tau(h,\lambda) = (b_{BrC}(h,\lambda) + b_{BC}(h,\lambda) + b_{Scat}(h,\lambda))\Delta h \quad (1)$$

where Δh represents the layer thickness centred at h, b_{BC} is the BC absorption coefficient, b_{BrC} is the BrC absorption coefficient, and b_{Scat} is the aerosol scattering coefficient. The SSA at altitude h and wavelength λ is computed as:

$$SSA(h,\lambda) = \frac{b_{BC}(h,\lambda) + b_{BrC}(h,\lambda)}{b_{BC}(h,\lambda) + b_{BrC}(h,\lambda) + b_{Scat}(h,\lambda)} \quad (2)$$

Aircraft measurements are used to compute the aerosol absorption and scattering coefficients in equations (1) and (2) (Supplementary Table 4). The wavelength-dependent aerosol absorption coefficients of BrC (b_{BrC}) are derived from measured solution absorption coefficients of BrC ($b_{SE,BrC}$) at 365 nm with the following equation:

$$b_{BrC}(\lambda) = b_{SE,BrC}(365\,nm) \times \left(\frac{\lambda}{365\,nm}\right)^{-AAE_{BrC}} \times f_{BrC} \quad (3)$$

where AAE_{BrC} is the absorption ångström exponent for BrC and f_{BrC} is the factor converting bulk solution absorption to aerosol absorption (see the Aircraft measurements section for more information about f_{BrC}). To account for the uncertainty in these parameters, we assign f_{BrC} a normal distribution with mean 2 and standard deviation 0.5 and a uniform distribution from 4.1 to 6.4 for AAE_{BrC} (refs 10,12) in the Monte Carlo computation. The range for AAE_{BrC} was derived using spectral information from the filter extract measurements and was found to show insignificant altitude dependence during DC3 (ref. 10).

The following equation computes the wavelength-dependent aerosol absorption coefficient of BC (b_{BC}) using the mass concentration (M_{BC}) measured by SP2:

$$b_{BC}(\lambda) = M_{BC} \times MAC_{BC}(660\,nm) \times \left(\frac{\lambda}{660\,nm}\right)^{-AAE_{BC}} \quad (4)$$

where AAE_{BC} is the absorption ångström exponent for BC and MAC_{BC} is the mass absorption cross-section for BC. We assign AAE_{BC} a uniform distribution from 0.8 to 1.2 (refs 14,40) and MAC_{BC} at 660 nm a normal distribution with mean 10 m^2 g^{-1} and standard deviation 4 m^2 g^{-1}. The numbers for MAC_{BC} are derived from the analysis using BC mass concentration and PSAP absorption at 660 nm, assuming BC is the only absorbing agent at 660 nm. The MAC of uncoated BC is recommended as 7.5 m^2 g^{-1} at 550 nm (ref. 41), which is 6.25 m^2 g^{-1} at 660 nm assuming $AAE_{BC} = 1$. Therefore, the mean MAC_{BC} (10 m^2 g^{-1}) used in our calculation is equivalent to a factor of 1.6 lensing effect, in agreement with the atmospheric relevant range suggested by previous studies[16,19].

Measurements from a three-wavelength (that is, 450, 550 and 700 nm) nephelometer are used to provide aerosol scattering information to the radiative transfer model. To account for the influence of hygroscopic growth on aerosol scattering, dry aerosol scattering at all three wavelengths is multiplied by the ratio of ambient aerosol scattering to dry aerosol scattering at 550 nm. Then, the wavelength-dependent aerosol scattering coefficients (b_{Scat}) are computed with the following equation:

$$b_{Scat}(\lambda) = b_{Scat}(550\,nm) \times \left(\frac{\lambda}{550\,nm}\right)^{-\frac{\ln\left(\frac{b_{Scat}(\lambda_0)}{b_{Scat}(550\,nm)}\right)}{\ln\left(\frac{\lambda_0}{550\,nm}\right)}} \quad (5)$$

where $\lambda_0 = 450$ nm when $\lambda < 550$ nm and $\lambda_0 = 700$ nm when $\lambda > 550$ nm.

Since the SBDART model outputs only the radiative imbalance at the top of the troposphere, to derive the radiative forcing, we conducted simulations with and without the agent in question and computed the radiative forcing of the agent as the difference of radiative imbalance between the two simulations. We gathered 1,000 samples from the Monte Carlo simulation and reported the mean and the standard deviation. The radiative forcing reported here is instantaneous direct forcing, assuming a zenith angle of 40°. To assess the influence of clouds, we conducted two sets of computation, one with clear sky and the other with the global-mean cloud distribution[42]. The RFs reported here are not directly comparable to the Intergovernmental Panel on Climate Change RF estimates, which are global and annual averages.

Uncertainties in radiative calculation. In this section, three major uncertainty sources for the BrC radiative calculation (that is, measurement/parameters, the size distribution of BrC, and the mixing state of BrC) are discussed.

Measurements and parameters. Using Monte Carlo simulations, we conduct additional analyses to further attribute the sources of uncertainty on the clear-sky calculation for DC3 (Table 1). For BrC, the horizontal inhomogeneity in BrC vertical profiles (0.09 W^2 m^{-4}) is responsible for 50% of the variation in the

computed RF due to BrC (0.18 $W^2\ m^{-4}$), followed by the uncertainty in f_{BrC} (36%), AAE_{BrC} (10%) and measurements (4%). For BC, the uncertainty in MAC_{BC} (1.8 $W^2\ m^{-4}$) accounts for 62% of the variation in the computed RF due to BC (2.9 $W^2\ m^{-4}$). The contributions from horizontal inhomogeneity and measurement uncertainty are 27% and 11%, respectively.

Size distribution of BrC. In our radiative calculation, we use a factor ($f_{BrC} \sim N(2, 0.5^2)$) to convert measured solution BrC absorption to aerosol BrC absorption, which stems mainly from the size effect of aerosols (that is, optical effects described by the Mie regime). According to the Mie calculation, a f_{BrC} close to 2 corresponds to a BrC median diameter of 0.5 μm (ref. 9), and is in agreement with several closure analyses using field measurements[7,9,10,31]. However, it is reasonable to speculate that the size distribution of BrC may have changed before and after convective processing, which can influence the value of f_{BrC}. Ref. 25 did show that a substantial fraction of fine mode (0.1–1 μm diameter) was removed during convection while the coarse mode (1–5 μm diameter) tended to remain. Unfortunately, we do not have size-resolved BrC data to verify if the size distribution of BrC follows the bulk aerosols.

To quantify this uncertainty, we conducted an additional radiative calculation, in which we assume the median diameter of high-altitude (>5 km) is 2 μm. According to Mie calculations, this corresponds to a f_{BrC} of 1.35. Results show that the smaller f_{BrC} for high-altitude BrC reduces the direct RF by high-altitude BrC absorption from 0.65 to 0.45 W m^{-2}, indicating that the size dependence of f_{BrC} may be an important source of uncertainty. However, the main conclusion that high-altitude BrC is a major contributor to the direct RF by BrC (57% in this calculation versus 65% if $f_{BrC} = 2$ throughout the column) is unchanged.

Mixing state. The RF can also be affected by the mixing state between BC, BrC and other aerosol components. Using model simulations with varied mixing state configurations, a recent study showed the nonlinear interplay between BrC absorption and the so-called lensing effect to be significant[19]. Instead of extensive modelling treatment for the mixing state as in ref. 19, our approach in this study is to use empirically determined parameters (MAC_{BC} and f_{BrC}) to account for the influence of mixing state on the RF calculations.

First, we use the total light absorption at 660 nm (measured by the PSAP) and BC mass concentration (measured by the SP2) data from the DC3 campaign to calculate the mean MAC_{BC} at 660 nm, assuming all the absorption at 660 nm is due to BC. On the basis of a linear regression fit, this results in a campaign-mean MAC_{BC} of 10 $m^2\ g^{-1}$ at 660 nm. In comparison to the measured MAC of uncoated BC (7.5 $m^2\ g^{-1}$ at 550 nm and 6.25 $m^2\ g^{-1}$ at 660 nm), our MAC_{BC} is equivalent to a factor of 1.6 enhancement of absorption due to lensing, falling in the atmospherically relevant range suggested by ref. 19.

Second, we use a factor ($f_{BrC} \sim N(2, 0.5^2)$) to convert measured solution BrC absorption to aerosol BrC absorption. Careful closure analyses against PSAP measurements in multiple field studies all support f_{BrC} to be close to 2 (refs 7,9,10,31). The closure in the field data indicates that the conversion factor has accounted for the size effect (the Mie effect) and, if any, the nonlinear effect due to BrC coating on BC.

Satellite products. We compare the AAOD derived from DC3 and SEAC^{4}RS with satellite retrieval products (OMI OMAERUVd v003) at 388 and 500 nm. The 1° × 1° data are obtained from the NASA Giovanni data portal (http://giovanni.gsfc.nasa.gov/giovanni). To compare with aircraft measurements, we average the satellite data during the DC3 (or SEAC^{4}RS) campaign over the corresponding regions in Supplementary Fig. 1. The averaging is weighted by the number of aircraft observations in sub-regions of Supplementary Fig. 1. Figure 1c and Supplementary Fig. 4a show that satellite-retrieved AAOD and wavelength dependence between 388 and 500 nm are in good agreement with aircraft observations in both DC3 and SEAC^{4}RS. Although uncertainties associated with satellite retrieval of AAOD are generally thought to be quite large[43], the interesting agreement between aircraft observations and satellite retrievals may partially result from good sensitivities of satellite observations to high-altitude absorption, suggesting that the satellite retrieval product can be useful to capture regional features of BrC[43–45].

We also use the Global Fire Emission Database Version 4s (GFED4s) to show that both DC3 and SEAC^{4}RS campaigns were under the influence of substantial biomass-burning emissions (Supplementary Fig. 2). GFED4s fire emissions are based on both satellite information and vegetation productivity. We obtain the data from www.globalfiredata.org/data.html and the horizontal resolution of the data is 0.25° × 0.25°.

Code availability. The code used to generate the radiative forcings is available from the authors on request.

Data availability. The DC3 data can be found at https://www-air.larc.nasa.gov/missions/dc3-seac4rs and the SEAC^{4}RS data at https://www-air.larc.nasa.gov/missions/seac4rs. The data supporting the findings of this study are also available from the corresponding author.

References

31. Washenfelder, R. A. *et al*. Biomass burning dominates brown carbon absorption in the rural southeastern United States. *Geophys. Res. Lett.* **42,** 653–664 (2015).
32. Schwarz, J. P. *et al*. Aircraft measurements of black carbon vertical profiles show upper tropospheric variability and stability. *Geophys. Res. Lett.* **44,** 1132–1140 (2017).
33. DeCarlo, P. F. *et al*. Field-deployable, high-resolution, time-of-flight aerosol mass spectrometer. *Anal. Chem.* **78,** 8281–8289 (2006).
34. Bond, T. C., Anderson, T. L. & Campbell, D. Calibration and intercomparison of filter-based measurements of visible light absorption by aerosols. *Aerosol Sci. Technol.* **30,** 582–600 (1999).
35. Virkkula, A. Correction of the calibration of the 3-wavelength particle soot absorption photometer (3λ PSAP). *Aerosol Sci. Technol.* **44,** 706–712 (2010).
36. Anderson, T. L. & Ogren, J. A. Determining aerosol radiative properties using the TSI 3563 integrating nephelometer. *Aerosol Sci. Technol.* **29,** 57–69 (1998).
37. Bela, M. M. *et al*. Wet scavenging of soluble gases in DC3 deep convective storms using WRF-Chem simulations and aircraft observations. *J. Geophys. Res.* **121,** 4233–4242 (2016).
38. Barth, M. C. *et al*. Convective transport and scavenging of peroxides by thunderstorms observed over the central US during DC3. *J. Geophys. Res.* **121,** 4272–4295 (2016).
39. Ricchiazzi, P., Yang, S., Gautier, C. & Sowle, D. SBDART: a research and teaching software tool for plane-parallel radiative transfer in the earth's atmosphere. *Bull. Am. Meteorol. Soc.* **79,** 2101–2114 (1998).
40. Olson, M. R. *et al*. Investigation of black and brown carbon multiple-wavelength-dependent light absorption from biomass and fossil fuel combustion source emissions. *J. Geophys. Res.* **120,** 6682–6697 (2015).
41. Bond, T. C. & Bergstrom, R. W. Light absorption by carbonaceous particles: an investigative review. *Aerosol Sci. Technol.* **40,** 27–67 (2006).
42. Zarzycki, C. M. & Bond, T. C. How much can the vertical distribution of black carbon affect its global direct radiative forcing? *Geophys. Res. Lett.* **37,** L20807 (2010).
43. Jethva, H., Torres, O. & Ahn, C. Global assessment of OMI aerosol single-scattering albedo using ground-based AERONET inversion. *J. Geophys. Res.* **119,** 9020–9040 (2014).
44. Jethva, H. & Torres, O. Satellite-based evidence of wavelength-dependent aerosol absorption in biomass burning smoke inferred from Ozone Monitoring Instrument. *Atmos. Chem. Phys.* **11,** 10541–10551 (2011).
45. Torres, O. *et al*. Aerosols and surface UV products from Ozone Monitoring Instrument observations: an overview. *J. Geophys. Res.* **112,** D24S47 (2007).